

Two Tasks, One Goal: Uniting Motion and Planning for Excellent End To End Autonomous Driving Performance

Lin Liu, Ziyong Song, Hongyu Pan, Lei Yang, Caiyan Jia

Abstract—End-to-end autonomous driving has made impressive progress in recent years. Former end-to-end autonomous driving approaches often decouple planning and motion tasks, treating them as separate modules. This separation overlooks the potential benefits that planning can gain from learning out-of-distribution data encountered in motion tasks. However, unifying these tasks poses significant challenges, such as constructing shared contextual representations and handling the unobservability of other vehicles' states. To address these challenges, we propose TTOG, a novel two-stage trajectory generation framework. In the first stage, a diverse set of trajectory candidates is generated, while the second stage focuses on refining these candidates through vehicle state information. To mitigate the issue of unavailable surrounding vehicle states, TTOG employs a self-vehicle data-trained state estimator, subsequently extended to other vehicles. Furthermore, we introduce ECSA (equivariant context-sharing scene adapter) to enhance the generalization of scene representations across different agents. Experimental results demonstrate that TTOG achieves state-of-the-art performance across both planning and motion tasks. Notably, on the challenging open-loop nuScenes dataset, TTOG reduces the L2 distance by 36.06%. Furthermore, on the closed-loop Bench2Drive dataset, our approach achieves a 22% improvement in the driving score (DS), significantly outperforming existing baselines.

Index Terms—End-to-End Autonomous Driving, Motion Prediction, Plan, Bird's-Eye-View.



1 INTRODUCTION

With the rapid development of deep learning, autonomous driving technology is evolving from traditional handcrafted, modular architectures towards end-to-end architectures. Unlike conventional methods that process multiple sub-tasks separately, end-to-end autonomous driving systems strive to seamlessly integrate and jointly optimize multiple sub-tasks. These systems take sensor data as input and directly output future trajectories or control signals. Owing to their holistic optimization capabilities and the advantage of avoiding error accumulation across modules, end-to-end autonomous driving algorithms have achieved significant progress [1, 2, 3, 4, 5, 6, 7, 8, 9], recently. As a critical input to the planning task, motion prediction's performance directly impacts the accuracy and robustness of planning outcomes. The most advanced methods currently use a serial structure [1, 3, 4] to connect the motion module and the plan module, or design both as parallel structures [2].

Such serial or parallel designs not only limit deep information interaction between tasks but may also lead to error propagation and performance bottlenecks, failing to fully exploit the synergistic potential between the two tasks.

Recently, some end-to-end autonomous driving works have attempted to integrate inputs from both planning and motion tasks [8, 10, 11, 12, 13, 14, 15, 16] and design complex interaction modules to simulate real-world task interactions. However, these methods often rely on heavily handcrafted rules or intricate structures, failing to fully exploit the intrinsic relationships between tasks. In this paper, we propose **TTOG**, a novel approach that redefines the planning task as a special case of motion prediction. This allows the planning task to be trained using data from other vehicles, enabling it to learn scenarios not encountered by the ego vehicle in the dataset. A straightforward approach is to train a unified decoder that does not distinguish between other vehicles and the ego vehicle, simultaneously performing predictions for both motion and planning tasks, thereby enabling the reuse of motion data. By sharing decoder parameters, this method can directly transfer knowledge from other vehicles' data to the ego vehicle's planning task. However, reusing motion data for the planning task faces two critical challenges. First, the ego state of other vehicles is inherently unavailable, leading to data incompleteness when directly training with motion data. Second, the input to the planning task is typically collected from the ego vehicle's perspective, while motion data is observed from other vehicles' perspectives. This perspective discrepancy results in significant inconsistencies in data distribution and contextual representation.

To address the aforementioned challenges, our model design is based on two key components:

Equivariant Context-Sharing Scene Adapter: To ensure that the extracted scene features are invariant to rotation and translation while enabling efficient sharing across multiple

- Z. Song, L. Liu, and C. Jia are with Beijing Key Laboratory of Traffic Data Mining and Embodied Intelligence, Beijing Jiaotong University. Email: {songziyong, 23120379, cyjia}@bjtu.edu.cn. Z. Song contributed to this work as an intern at Horizon Robotics.
- H. Pan is with Horizon Robotics. Email: karry.pan@horizon.cc.
- Y. Luo is with School of Information Technology and Electrical Engineering, The University of Queensland, Australia. Email: y.luo@uq.edu.au.
- L. Yang is with School of Vehicle and Mobility, Tsinghua University, China. Email: yanglei20@mails.tsinghua.edu.cn.

Corresponding author: Caiyan Jia.

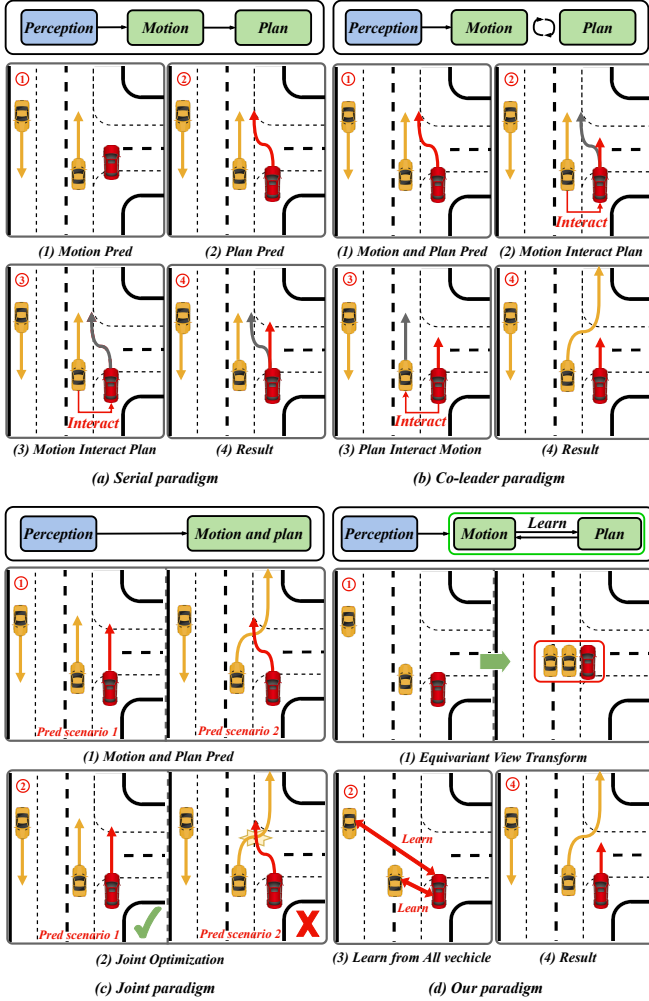


Fig. 1: (a) **Serial Paradigm** [1, 4, 17, 18, 19, 20, 21, 22] serves the output of the motion prediction module as a prior condition for the planning task. So it relies on the assumption that the ego vehicle will prioritize yielding to others, leading to overly conservative driving strategies. (b) **Co-leader Paradigm** [10, 11, 12, 13, 14, 23] aims to independently construct motion and planning modules while establishing an iterative interaction mechanism between them. However, such paradigm struggle to effectively utilize motion data as training exemplars, thereby creating data underutilization issues. (c) **Joint Paradigm** [8, 15, 24] aims to simultaneously output motion and planning results. This paradigm is founded on the assumption that a globally optimal outcome exists for both the EV and SVs collectively. Specifically, the EV’s trajectory is derived through a global optimization process involving all agents. However, these methods are predicated on the assumption that the behavioral and state models of the SV are fully known. (d) **Our Paradigm** is designed to unify both ego-vehicle data and other-vehicle data into a unified perspective, enabling joint learning and training. This approach allows the planning task to fully benefit from trajectory data of other vehicles, thereby enhancing the model’s generalization capability and robustness in few-shot scenarios.

agents, TTOG integrates an Equivariant Graph Neural Network with a Set Attention Mechanism to construct the scene encoder. Specifically, TTOG adopts a hierarchical graph representation framework to model multi-agent interactions. From the ego vehicle’s perspective, agents are clustered into distinct groups, with each group represented as a subgraph. These subgraphs are processed through an Equivariant Graph Neural Network (EGNN) to capture local equivariant relationships. Subsequently, all nodes within each subgraph are aggregated into a single global node, representing the group’s collective state. These global nodes then form a higher-level global graph, which is further processed by EGNN to learn comprehensive global interactions. The updated global nodes propagate information back to each node in the subgraphs through a set-based self-attention mechanism, enabling recursive global relationship dissemination and facilitating adaptive intra-group interactions.

Unified Two-Stage Trajectory Decoder: To address data modality missing and enable parameter sharing of the trajectory decoder between motion and planning tasks, we decouple the planning task into two sub-tasks: *1) Trajectory Proposal Generation*, Leveraging the result from online mapping task, TTOG generates diverse trajectory proposals for the ego vehicle, which are fused with scene information and decoded. In addition to supervising the L2 deviation between predicted and ground truth trajectories, TTOG treats the proposals as pseudo-labels and supervises their distributional difference with predicted trajectories, promoting multimodal trajectory outputs. *Trajectory Filtering and Optimization*, The candidate trajectories from the first stage are encoded and fused with the ego vehicle’s state, followed by filtering and optimization in the second stage to derive the final planned trajectory. During training, TTOG unifies the first stage of motion and planning, while training an ego state predictor to estimate the current state based on historical ego states and scene context. During testing, TTOG extends this predictor to other vehicles, achieving full unification of motion and planning predictions.

Overall, our contributions are as follows:

- TTOG introduces a novel approach to unify motion and planning tasks, enabling the planning task to benefit from motion data. This significantly enhances the performance and generalization capability of the planning task.
- To address the inconsistency in data perspectives between motion and planning tasks, TTOG propose the **Equivariant Context-Sharing Scene Adapter (ECSA)**. This adapter leverages an Equivariant Graph Neural Network (E-GNN) and a Set Attention Mechanism to extract rotation- and translation-invariant scene features from multi-agent interactions, enabling highly shared and consistent scene representations across agents.
- To address the inconsistency in data modalities between motion and planning tasks, we propose a **Unified Two-Stage Trajectory Decoder (UTTD)**. This decoder decomposes the planning task into two sub-tasks and incorporates an additional vehicle state estimator, enabling parameter sharing between motion and planning decoders.
- Extensive experiments on the open-loop evalua-

tion dataset *nuScenes* and the closed-loop dataset *Bench2Drive* demonstrate the effectiveness of our method. TTOG achieves significant improvements, reducing L2 displacement error by 22% and increasing the driving score by 34%.

2 RELATED WORK

2.1 End-to-end Autonomous Driving

End-to-end autonomous driving directly maps raw sensor inputs data to future ego-vehicle trajectories, eliminating handcrafted rules. Early approaches [25, 26, 27, 28, 29] often employed process-implicit architectures without auxiliary task supervision (e.g., detection, online mapping, motion prediction), resulting in poor interpretability and optimization difficulties. Close-loop-based methods [7, 9, 29, 30, 31, 32, 33] learn vehicle actions in closed-loop simulations but struggle with the sim scene to real scene distribution gap, limiting their practical applicability.

Recent methods [1, 3, 4, 6, 8, 30, 34, 35, 36, 37, 38, 39, 40], such as UniAD [1], integrate perception, prediction, and planning modules for trajectory optimization, achieving state-of-the-art performance. VAD [3] introduced vectorized scene representations with explicit planning constraints, while VADv2 [4] enhanced diversity via multi-modal trajectories. GraphAD [40] modeled dynamic-static interactions via scene graphs, and PPAD [34] iteratively refined motion and planning outputs. SparseDrive [2] incorporated symmetric sparse perception but lacked motion-planning interaction, a limitation addressed by DiFSD [14]. Despite their advancements, these methods fail to leverage motion data for planning, missing opportunities to learn from out-of-distribution scenarios. Our UniMP explicitly tackles this gap.

2.2 Integration of Motion and Planning

Traditional modular autonomous driving systems typically treat prediction and planning as sequential, independent tasks. While this accounts for the influence of surrounding traffic on the ego vehicle, it fails to model how traffic participants react to the ego vehicle’s behavior. Recent methods increasingly integrate prediction and planning into joint or interdependent steps. In this section, we categorize the Integration of Motion and Planning into three classes for review:

1) **Serial Integration.** Serial integration [1, 4, 17, 18, 19, 20, 21, 22?] executes planning and motion as separate tasks connected through differentiable interfaces, enabling end-to-end training. Typically, the output of the motion prediction module serves as a prior condition for the planning task. While this approach partially models interactions between the ego vehicle and other agents, it relies on the assumption that the ego vehicle will prioritize yielding to others, leading to overly conservative driving strategies.

2) **Co-leader Integration.** The co-leader integration framework aims to independently construct motion and planning modules while establishing an iterative interaction mechanism between them. This approach models the

influence of SVs’ (Surrounding Vehicles) potential future behaviors on the EV’s (Ego Vehicle) planning and its stochastic responses to alternative ego trajectories. DTPP [41] extends this framework with a Transformer-based conditional prediction module, enabling simultaneous predictions of all agents conditioned on multiple EV plans. Some approaches [10, 11, 12, 13] endeavor to model the potential impact of multiple SV trajectories within a single frame on the selection of the EV’s trajectory, thereby minimizing the probability of future collisions to hedge against worst-case risks. Alternative approaches [14, 23] focus on constructing iterative interaction mechanisms to recursively optimize motion and planning outcomes. DiFSD [14] re-feeds the planning results, conditioned on motion outputs, as prior constraints for the next iteration of motion planning. DriveWorld [23] leverages a world model to estimate the reciprocal influences between ego and other vehicles’ trajectories, followed by trajectory refinement.

3) **Joint Integration.** The Joint Integration paradigm aims to simultaneously output motion and planning results. This paradigm is founded on the assumption that a globally optimal outcome exists for both the EV and SVs collectively. Specifically, the EV’s trajectory is derived through a global optimization process involving all agents. As a pioneering work, Gameformer [15] simultaneously outputs motion and planning results, modeling their interactions as a level-k game [16], where the decoder iteratively updates individual predictions based on the anticipated behaviors of all agents from the previous layer to simulate inter-agent interactions. Similarly, SafePathNet [24] employs transformers for joint prediction and planning, subsequently ranking them based on estimated probabilities and collision avoidance. The recent end-to-end approach, GenAD [8], adopts an autoregressive generative decoder to jointly regress SV and EV trajectories. However, these methods are predicated on the assumption that the behavioral and state models of the SV are fully known. In contrast, UniMP introduces an alternative approach by pretraining the planning task using motion data, enabling the planning task to benefit from the motion task, while also addressing the challenge of acquiring SV states.

3 METHOD

Fig. 2 illustrates the architecture of the proposed TTOG, which introduces a novel end-to-end paradigm integrating motion prediction and trajectory planning. This framework enables comprehensive knowledge transfer from motion data to enhance planning performance through joint learning. The core innovations consist of two principal components: 1) **Equivariant Context-Sharing Scene Adapter** (Sec 3.1), which represents traffic agents and map elements as graph nodes, dynamically partitioning them into subgraph groups and preserving global topology through inter-subgraph connections. An equivariant graph neural network subsequently processes hierarchical graph structures, where multi-scale relationships are learned through propagates cross-group interactions to maintain geometric equivariance. 2) **Unified Two-Stage Trajectory Decoder** (Sec ??), The decoding process comprises, *proposal generation stage* (Sec 3.2.2): Produces multi-modal trajectory hypotheses

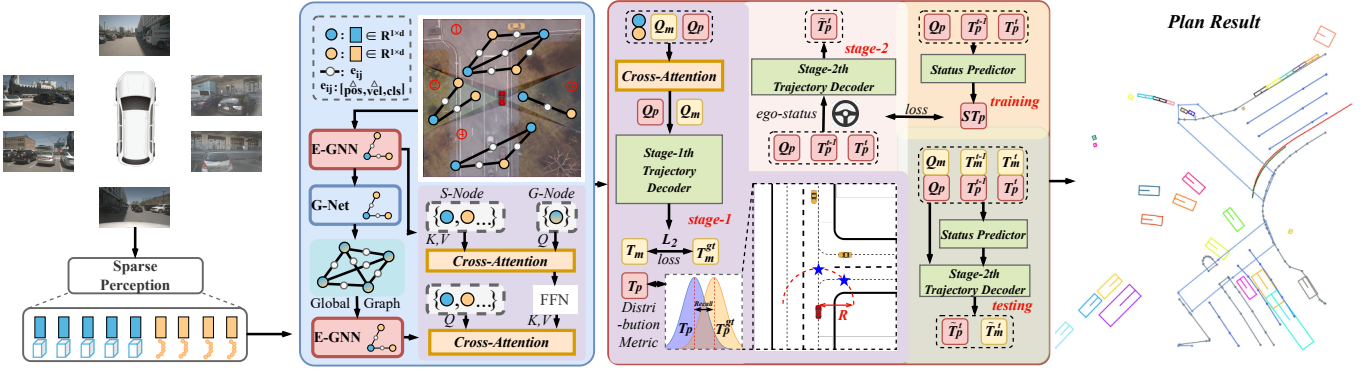


Fig. 2: **The overall architecture of TTOG.** TTOG follows SparseDrive and encodes multi-view images into feature maps, then represents the sparse scene as a composition of map instances and agent instances through sparse perception. (a) ECSA models traffic agents and map elements as graph nodes, dynamically grouping them into subgraphs while preserving global topology via inter-subgraph connections. An equivariant GNN then processes this hierarchical structure, learning multi-scale relationships through cross-group interactions to maintain geometric equivariance. (b) UTTD unifies motion and planning trajectory prediction through a two-stage framework: proposal generation and likelihood-aware refinement. During inference, an auxiliary vehicle state estimator is applied to other vehicles to address missing data modalities.

conditioned on structured scene graphs. *Likelihood-Aware refinement stage* (Sec 3.2.2): Executes context-aware trajectory optimization by integrating ego-state dynamics. To enable unified prediction, an auxiliary Ego-State Predictor is trained using historical observations and environmental contexts. During inference, this probabilistic estimator is symmetrically applied to all agents, achieving unified motion forecasting and ego-planning within the same geometric learning framework.

3.1 Equivariant Context-Sharing Scene Adapter

In this work, TTOG adopts a more compact and explicit representation of the semantic scene, thereby abandoning the BEV representation. Instead, TTOG constructs an equivariant scene graph based on the sparse perception results of SparseDrive. Following the tasks of detection and online mapping, both the agent and map elements are represented as $\{F_a \in \mathbb{R}^{N_a \times C}, B_a \in \mathbb{R}^{N_a \times 11}\}$ and $\{F_m \in \mathbb{R}^{N_m \times C}, L_m \in \mathbb{R}^{N_m \times N_p \times 2}\}$. F_a and F_m denote the features of the agent and map elements, respectively. B_a represents the detection box, formatted with parameters including location, dimension, yaw angle, and velocity. L_m signifies the anchor polylines. The centroids of map elements' polyline and the agents are denoted as $Cer = \{Cer_m \in \mathbb{R}^{N_m \times 3}, Cer_a \in \mathbb{R}^{N_a \times 3}\}$.

To enhance the model's processing efficiency, TTOG constructs hierarchical subgraphs to learn equivariant scene representations. The scene is partitioned into four regions based on the human driver's attention range and the ego vehicle's heading angle: Forward Zone ($+30^\circ$ to $+150^\circ$), Lateral Zones (-30° to $+30^\circ$ and 150° to 210°), and the rearward zone (-30° to -150°). The ego vehicle is replicated into four instances, each assigned to one of these zones. The high-level approach for computing edge connections within each group involves calculating pairwise distances between graph nodes and connecting each node to its K nearest neighbors. Furthermore, a node gv_i is added to each subgraph, with its position determined by the mean coordinates of the nodes within the subgraph, and its features extracted from all constituent nodes using PointNet [42]. Initially,

TTOG focus on learning the equivariant relationships within the subgraphs. TTOG set a graph $G = (V, E)$ with nodes $v_i \in V$ and edges $e_{ij} \in E$, where the node features consist of F_a and F_m . Based EGCL [43], the node are updated as follows:

$$\begin{aligned} \Delta Cer_{ij} &= \left\| \phi_e(Cer_i^l) - \phi_e(Cer_j^l) \right\|, \\ m_{ij} &= g_e(v_i^l, v_j^l, \Delta Cer_{ij}, e_{ij}), \\ Cer_i^{l+1} &= Cer_i^l + C \sum_{j \neq i} \Delta Cer_{ij} \cdot g_x(m_{ij}), \\ v_i^{l+1} &= g_h(v_i^l, \sum_j m_{ij}). \end{aligned} \quad (1)$$

which g_e , g_x and g_h are multi-layer perceptions (MLPs). Here, ϕ_e is utilized for position encoding, while g_x , g_x and g_e are employed for feature projection.

$$\begin{aligned} r_{ij} &= [vel_i - vel_j, cls_i^v, cls_j^v] \\ e_{ij} &= MLP(r_{ij}) \end{aligned} \quad (2)$$

Here, vel represents the node velocity, with the vel of map nodes set to zero. Additionally, the extra node gv_i is derived from the vector sum of other nodes' velocities $\sum vel_i$, while cls_i^v denotes the node category. The nodes of the subsequent global graph are denoted as $GV = \{gv_i | i = 1, 2, \dots, N_{gv}\}$, $N_{gv} = 4$. Any two nodes are connected by an edge, where the initial attribute of e_{ij} is solely characterized by $\{vel_i - vel_j\}$, thereby excluding node categories cls_i . The global graph adheres to the operation defined in Eq. 1 to learn equivariant relations.

Following the equivariant graph neural network as shown in formula 1, TTOG obtain the updated subgraph node features V and global graph node features GV . Subsequently, for each subgraph's node set V_i and the global node GV_i , TTOG utilize a set self-attention mechanism to propagate the learned global relations back to the subgraph nodes, facilitating both the updating of global relationships

and the intra-subgraph interactions among nodes, as shown in Eq. 1.

$$\begin{aligned}\hat{G}V_i &= \text{CrossAttn}(GV_i, V_i, V_i) \in \mathbb{R}^{1 \times d}, \\ \hat{G}V_i &= \text{FFN}(GV_i), \\ \hat{V}_i &= \text{CrossAttn}(V_i, \hat{H}, \hat{H}) \in \mathbb{R}^{k \times d}.\end{aligned}\quad (3)$$

Where, k denotes the number of nodes within a sub-graph, and d represents the feature dimensionality.

3.2 Unified Two-Stage Trajectory Decoder

To enable the sharing of trajectory decoder parameters across motion and planning tasks with heterogeneous data modalities, thereby facilitating knowledge transfer, TTOG introduces a Unified Two-Stage Trajectory Decoder architecture.

3.2.1 Proposal Generation Stage

In Stage I, TTOG refrains from incorporating the ego vehicle state, instead predicting all potential trajectories for the ego vehicle in the same manner as it forecasts those for surrounding vehicles. This process, termed the trajectory candidate generation stage, leverages cross-attention mechanisms between the motion query $Q_m \in \mathbb{R}^{N_m \times d}$ and plan query $Q_p \in \mathbb{R}^{N_p \times d}$, as well as agent and map elements, to achieve comprehensive information fusion. The integrated Q and M features are processed by the first-stage trajectory decoder to produce the preliminary trajectory estimation:

$$\begin{aligned}\{Q_m, Q_p\} &= \text{CrossAttn}(\{Q_m, Q_p\}, V, V) \in \mathbb{R}^{(N_p+N_m) \times K \times d}, \\ \{T_m^{\text{pred}}, T_p^{\text{pred}}\} &= \text{TrDec}(\{Q_m, Q_p\}) \in \mathbb{R}^{(N_p+N_m) \times t_{\text{traj}} \times K \times 2}.\end{aligned}\quad (4)$$

The trajectory length, denoted as t_{traj} , is configured as 6 in the decoding stage. K denotes the num of trajectory proposals and is set to 6. In the first stage of trajectory supervision, L_2 loss is applied to motion-task trajectories and GT T_m^{gt} , while planning-task trajectories adopt a distribution-based metric. The GT for planning is derived as follows: at time t , with the ego vehicle's center p_{ego} as the origin, a semicircle of radius $vel \cdot t_{\text{traj}}$ is drawn along the motion direction. Its intersection with the center lane \mathcal{L}_c defines potential future positions, used as planning GT \tilde{T}_p^{gt} :

$$\tilde{T}_p^{\text{gt}} = \left\{ \mathbf{p} \mid \mathbf{p} \in \mathcal{L}_c, \|\mathbf{p} - \mathbf{p}_{\text{ego}}\|_2 = vel \cdot t_{\text{traj}} \right\} \quad (5)$$

$$loss_{1th}^{\text{plan}} = \mathbb{E}_{k < K} \left(\min_{k' < K_{gt}} \left\| \hat{T}_{p,k}^{\text{pred}} - \tilde{T}_{p,k'}^{\text{gt}} \right\|_2 \right) < d \quad (6)$$

Here, K_{gt} denotes the number of ground truth \tilde{T}_p^{gt} , $\tilde{T}_{p,k}^{\text{gt}}$ represents the k -th predicted value in \tilde{T}_p^{gt} , and k' signifies the k' -th ground truth in \tilde{T}_p^{gt} .

3.2.2 Likelihood-Aware Refinement Stage

In Stage II, distinct strategies are employed during training and testing. The training phase focuses exclusively on refining the ego-vehicle trajectory. Leveraging the multi-modal trajectory predictions and corresponding queries from the

first phase, the ego-vehicle state serves as the pivotal element for prediction, enabling precise trajectory optimization through the integration of these components:

$$\begin{aligned}T_p^{\text{pred}} &= \text{TrDec}(\{Q_p, ST_p, T_p^{\text{pred}}\}) \in \mathbb{R}^{N_p \times K \times t_{\text{traj}} \times 2}, \\ ST_p &= \min_f \left\| f(Q_p, T_p^{\text{his}}) - ST \right\|_2.\end{aligned}\quad (7)$$

In this context, ST denotes the ego vehicle's state. Notably, during the training process, an additional STP (*State Predictor*) is trained. This predictor takes the vehicle's historical trajectory T_p^{his} and features Q_p as input, outputs the predicted vehicle state, and is supervised by the ground truth ST for optimization. During the testing phase, the trained STP is utilized to unify motion and planning. Given the vehicle features and historical trajectory for the motion task, the two-stage trajectory prediction is formulated as:

$$\begin{aligned}T_m^{\text{pred}} &= \text{TrDec}(\{Q_m, STP(Q_m, T_m^{\text{his}}), T_m^{\text{pred}}\}), \\ T_m^{\text{pred}} &\in \mathbb{R}^{N_m \times K \times t_{\text{traj}} \times 2}\end{aligned}\quad (8)$$

In this manner, the motion and planning tasks achieve parameter sharing throughout the decoding process.

4 EXPERIMENTS

4.1 Experiments Setup

4.1.1 Datasets

For Open-Loop testing, TTOG conducted comprehensive experiments on the widely adopted open-loop benchmark dataset, NuScenes [44], encompassing tasks of detection, online mapping, motion prediction, and planning. The NuScenes dataset comprises 1,000 driving sequences, each spanning 20 seconds and containing 40 annotated key frames. Each data sample includes six images captured by surrounding cameras, providing a 360° field of view. Point clouds are collected by LiDAR and radar sensors. In our experiments, we exclusively utilized image data as model inputs, omitting LiDAR data.

For Close-Loop testing, TTOG was evaluated on the closed-loop benchmark dataset, Bench2Drive [45], for tasks including detection, online mapping, motion prediction, and planning. Bench2Drive is a large-scale expert dataset comprising both open-loop and closed-loop evaluations, featuring three distinct data partitions: *mini* (10 clips), *base* (100 clips), and *large* (10,000 clips). The open-loop training data consists of two million fully annotated frames, with each key sample annotated at 10 Hz, including 3D bounding boxes, depth, and semantic segmentation, which comprises sensor configurations including LiDAR, six Cameras, five Radars, an IMU/GNSS module, and a BEV Camera, integrated with HD map data. For closed-loop testing, Bench2Drive systematically collects data from 220 routes uniformly distributed across 44 interactive scenarios (such as lane cutting, overtaking, and detours), 23 weather conditions (including clear, foggy, and rainy conditions), and 12 distinct towns in CARLA v2 (encompassing urban, rural, and university environments).

For Few-shot testing, TTOG method offers a distinct advantage by leveraging motion data to augment scarce planning samples, thereby enhancing the performance of end-to-end approaches. To validate this, we curated two

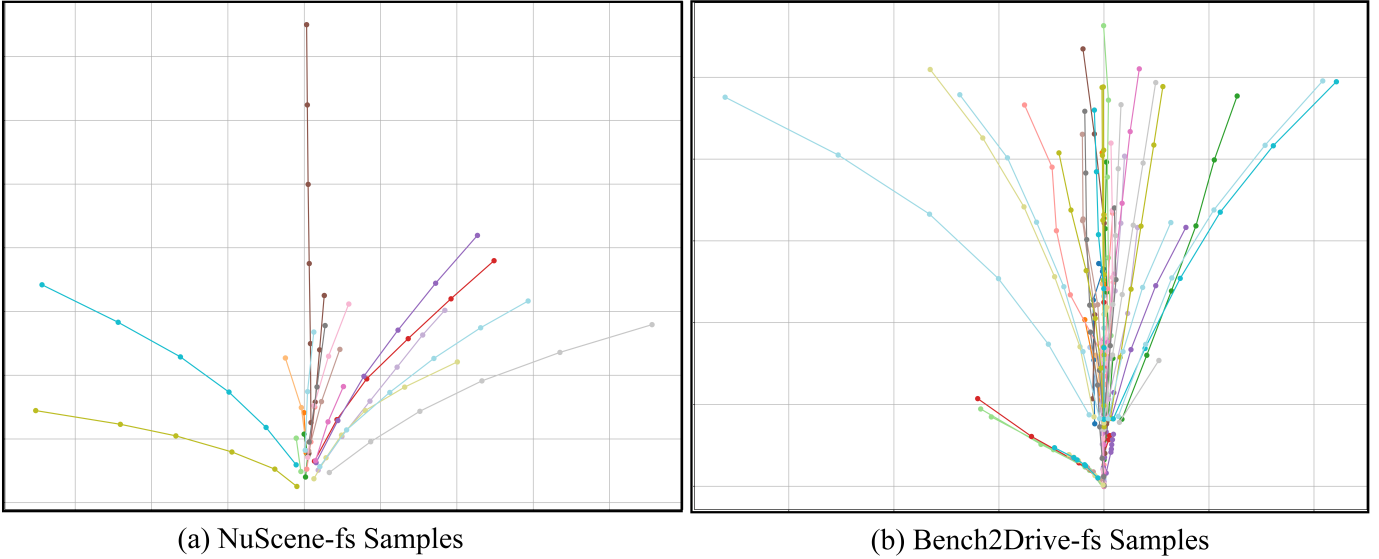


Fig. 3: For the ego trajectory visualization results in the NuScenes-FS and Bench2Drive-FS datasets, each ego trajectory is randomly sampled from its corresponding cluster. The NuScenes-FS dataset contains 32 clusters, while the Bench2Drive-FS dataset contains 62 clusters.

few-shot test datasets - nuScenes-fs and Bench2drive-fs - through the following systematic process: We applied the OPTICS adaptive clustering algorithm to ego-trajectories from the validation set, ranked the clusters by population size, and selected samples from the k smallest clusters to construct our few-shot datasets.

4.1.2 Evaluation Metrics for Planning

For open-loop planning evaluation, we employ conventional L_2 error and CR (collision rate) as metrics, aligning with the computation method of SparseDrive [2]. Regarding closed-loop planning assessment, we follow the Bench2Drive [45] dataset setting, measuring DS (Driving Score) and SR (Success Rate (%)). Additionally, we introduce a novel metric, CEGR (Cross-Vehicle Efficiency Gain Ratio), to assess motion data utilization efficiency and model convergence speed.

$$CEGR = \frac{(Acc - Acc_{base})}{(Acc_{base})} \cdot \left(1 - \frac{D_{ego}}{D_{ego+agent}}\right) \cdot 100\% \quad (9)$$

CEGR demonstrates the capability of effectively converting motion data into learnable representations for planning tasks. Here, Acc and Acc_{base} denote the performance of the proposed model and the baseline method, respectively. D_{ego} represents the training data volume for the ego vehicle, while D_{agent} denotes the training data volume for other vehicles.

4.1.3 Implementation Details

TTOG adopts SparseDrive [2] as its baseline framework and follows the two-stage training protocol established by SparseDrive. For nuScenes [44] dataset, we utilize 750 clips for training and 150 clips for validation. The first stage focuses on training detection and online mapping tasks, employing the learning rate of $3e-4$ for 80 epochs with

the batch size of 4. Subsequently, the second stage is dedicated to motion prediction and planning tasks, maintaining the same learning rate and batch size for 10 epochs. For Bench2Drive dataset [45], we conduct experiments using the base-scale configuration, allocating 950 clips for training and 50 clips for validation. To adapt for its distinct sampling frequency, we adjust the training schedule as follows: in the first stage, we employ the learning rate of $3e-4$ with a batch size of 4 for 8 epochs; In the second stage, we maintain the same learning rate and batch size for 2 epochs.

4.2 Main Result

4.2.1 Plan Results

In NuScenes (Open-Loop), Table 2 presents a comparative evaluation of various end-to-end methods in terms of L_2 distance error and collision rate. Our proposed method, TTOG, demonstrates state-of-the-art performance, significantly outperforming both LiDAR-based and Camera-based approaches across all evaluated metrics. Compared to our baseline method, SparseDrive [2], our TTOG method achieves a substantially lower L_2 error of 0.40 (m) and a reduced collision rate of 0.09%. This 34.42% reduction in L_2 error demonstrates the effectiveness of our approach in achieving more precise and safer trajectory predictions. Among SOTA camera-based methods like UniAD [1], VAD [3] and GenAD [8], our TTOG model outperforms them in both accuracy and safety. Besides, despite the inherent advantage of LiDAR in depth perception, TTOG surpasses all LiDAR-based methods (IL, NMP, FF, and EO) in both L_2 error and collision rate. This highlights the superiority of the TTOG’s ECSA module, which effectively compensates for the lack of camera depth information through robust feature extraction. For metrics CEGR,

In Bench2Drive (Open-Loop and Close-Loop), as shown in Table. 4, experimental results demonstrate that our proposed TTOG method achieves superior performance in both

TABLE 1: The detailed information about the NuScene-fs and Bench2drive-fs datasets, specifically details the selected scenarios and the corresponding number of samples per scenario. The "total" row in the table indicate the overall number of samples included in each dataset.

Dataset	Bench2Drive-fs	NuScene-fs
Exemplary scenario	HazardAtSideLane_Town10HD_Route373_Weather9:1 YieldToEmergencyVehicle_Town04_Route166_Weather10:62 HardBreakRoute_Town01_Route32_Weather6:123 SignalizedJunctionLeftTurnEnterFlow_Town13_Route657_Weather2:26 InterurbanActorFlow_Town12_Route1291_Weather1:6 InvadingTurn_Town02_Route95_Weather9:94 VanillaNonSignalizedTurnEncounterStopsign_Town12_Route979_Weather9:20 StaticCutIn_Town05_Route226_Weather18:107	scene-0269: 1, scene-0272: 3 scene-0274: 4, scene-0276: 6 scene-0221: 2, scene-0012: 1 scene-0014: 4, scene-0015: 4 scene-0036: 4, scene-0038: 3 scene-0092: 3, scene-0093: 1 scene-0097: 7, scene-0098: 1 scene-0101: 7, scene-0102: 3
	Total	1838

TABLE 2: Planning results on the nuScenes [44] validation dataset. † denotes evaluation protocol used in UniAD [1]. * denotes results reproduced with the official checkpoint.

Method	Input	Backbone	L2 (m) ↓				Col. Rate (%) ↓				CEGR (%) ↓				FPS ↑
			1s	2s	3s	Avg.	1s	2s	3s	Avg.	1s	2s	3s	Avg.	
IL [46]	LiDAR	VoxelNet	0.44	1.15	2.47	1.35	0.08	0.27	1.95	0.77	-	-	-	-	-
NMP [47]	LiDAR	VoxelNet	0.53	1.25	2.67	1.48	0.04	0.12	0.87	0.34	-	-	-	-	-
FF [48]	LiDAR	VoxelNet	0.55	1.20	2.54	1.43	0.06	0.17	1.07	0.43	-	-	-	-	-
EO [49]	LiDAR	VoxelNet	0.67	1.36	2.78	1.60	0.04	0.09	0.88	0.33	-	-	-	-	-
ST-P3 [50]	Camera	ResNet50	1.33	2.11	2.90	2.11	0.23	0.62	1.27	0.71	-	-	-	-	1.6 (RTX3090)
OccNet [51]	Camera	ResNet50	1.29	2.13	2.99	2.14	0.21	0.59	1.37	0.72	-	-	-	-	2.6 (RTX3090)
UniAD [1]	Camera	ResNet101	0.45	0.70	1.04	0.73	0.62	0.58	0.63	0.61	0.41	0.68	0.97	0.68	1.8 (A100)
VAD [3]	Camera	ResNet50	0.41	0.70	1.05	0.72	0.03	0.19	0.43	0.21	0.36	0.66	0.91	0.64	-
GenAD [8]	Camera	ResNet50	0.36	0.83	1.55	0.91	0.06	0.23	1.00	0.43	-	-	-	-	6.7 (RTX3090)
SparseDrive [2]	Camera	ResNet50	0.29	0.58	0.96	0.61	0.01	0.05	0.18	0.08	0.30	0.57	0.85	0.57	9.0 (RTX4090)
TTOG (Ours)	Camera	ResNet50	0.16	0.38	0.69	0.39	0.01	0.03	0.14	0.06	0.30	0.53	0.78	0.54	6.4 (RTX4090)

TABLE 3: Planning results on the NuScene-FS validation dataset and Bench2Drive-FS validation dataset. TTOG . Red indicates improvement.

Method	NuScene-FS								Bench2Drive-FS							
	L2 (m) ↓				Col (%) ↓				L2 (m) ↓				Col (%) ↓			
	1s	2s	3s	avg	1s	2s	3s	avg	1s	2s	3s	avg	1s	2s	3s	avg
UniAD [1]	-	-	-	-	-	-	-	-	-	-	-	-	-	-	-	-
VAD [3]	0.45	0.81	2.34	1.20	0.05	0.27	1.09	0.47	0.55	1.20	2.36	1.37	0.00	0.00	0.00	0.00
SparseDrive [2]	0.29	0.59	0.99	0.63	0.00	0.00	0.29	0.09	0.47	0.82	1.68	0.98	0.00	0.00	0.00	0.00
TTOG	0.15	0.39	0.80	0.45	0.00	0.00	0.09	0.03	0.41	0.75	1.31	0.84	0.00	0.00	0.00	0.00
+improvement	<i>-0.14</i>	<i>-0.20</i>	<i>-0.19</i>	<i>-0.18</i>	<i>-0.00</i>	<i>-0.00</i>	<i>-0.20</i>	<i>-0.06</i>	<i>-0.06</i>	<i>-0.07</i>	<i>-0.37</i>	<i>-0.00</i>	<i>-0.00</i>	<i>-0.00</i>	<i>-0.00</i>	<i>-0.00</i>

open-loop and closed-loop evaluations. Compared to the SparseDrive [2] baseline, TTOG significantly reduces the average L2 error (open-loop metric) from 0.83m to 0.74m, indicating more accurate trajectory prediction. For closed-loop metrics, TTOG outperforms SparseDrive [2] with a Driving Score improvement from 42.12 to 45.23 and Success Rate increase from 15.10% to 16.01%. Furthermore, TTOG surpasses state-of-the-art methods (UniAD [1] and VAD [3]) across all evaluation metrics.

Besides, as shown in Table. 5, we evaluate the performance of state-of-the-art E2E autonomous driving methods on the Bench2Drive benchmark, assessing key driving abilities including Merging, Overtaking, Emergency Brake, Give Way, and Traffic Sign recognition. The compared methods include AD-MLP [38], UniAD-Tiny [1], UniAD-Base [1], VAD [3], SparseDrive [2] (baseline), and our proposed ap-

proach, TTOG. The experimental results demonstrate that TTOG consistently surpasses the baseline across all evaluated metrics, achieving relative improvements of 16.18% in Merging, 24.29% in Overtaking, and 20.00% in Emergency Brake. Notably, TTOG exhibits significant gains in Give Way (21.50%) and Traffic Sign recognition (23.03%), culminating in a mean performance of 21.12% a substantial advancement over SparseDrive’s 18.60%.

The superior performance of TTOG stems from its novel integration of motion-aware unified training, which enables joint optimization across diverse planning tasks. Unlike existing approaches that treat driving subtasks independently, TTOG leverages motion priors to enhance generalization, resulting in a more robust and adaptive autonomous driving system. This unified learning paradigm not only improves task-specific performance but also ensures scalability across

TABLE 4: Open-loop and Closed-loop Results of E2E-AD Methods in Bench2Drive [45]. Avg. L2 is averaged over the predictions in 2 seconds under 2Hz. * denotes results reproduced with the official checkpoint.

Method	Input	Open-loop Metric			Close-loop Metric	
		Avg. L2(m) ↓			Driving Score↑	Success Rate↑
UniAD-Tiny [1]	Ego State + 6 Cameras	0.80			32.00	9.54
UniAD-Base [1]	Ego State + 6 Cameras	0.73			37.72	9.54
VAD [3]	Ego State + 6 Cameras	0.91			39.42	10.00
AD-MLP [38]	Ego State	3.64			9.14	0.00
SparseDrive* [2]	Ego State + 6 Cameras	0.83			42.12	15.00
TTOG	Ego State + 6 Cameras	0.74			45.23	16.36

TABLE 5: Multi-Ability Results of E2E-AD Methods in Bench2Drive Dataset. * denotes results reproduced with the official checkpoint.

Method	Ability(%)					
	Merging	Overtaking	Emergency Brake	Give Way	Traffic Sign	Mean
AD-MLP [38]	0.00	0.00	0.00	0.00	4.35	0.00
UniAD-Tiny [1]	8.89	9.33	20.00	20.00	15.43	14.73
UniAD-Base [1]	14.10	17.78	21.67	10.00	14.21	15.55
VAD [3]	8.11	24.44	18.64	20.00	19.15	18.07
SparseDrive* [2]	12.50	17.50	20.00	20.00	23.03	18.60
TTOG	16.18	24.29	20.00	21.50	23.03	21.12

TABLE 6: Ablation studies of the impact of the different modules in TTOG on the NuScenes [44] and Bench2Drive [45] validation datasets. UMP stands for the unified output of motion and planning in a simplified manner. ECSA denotes Equivariant Context-Sharing Scene Adapter module, TTOG denotes Unified Two-Stage Trajectory Decoder. **Blue** represents positive improvement, and **Red** represents negative improvement.

UMP	ECSA	UTTD	NuScene									Bench2Drive																													
			L2(m) ↓			Col.Rate(%) ↓			CEGR(L2) ↑			L2(m) ↓			Col.Rate(%) ↓			CEGR(L2) ↑																							
			2s	3s	Avg	2s	3s	Avg	2s	3s	Avg	2s	3s	Avg	2s	3s	Avg	2s	3s	Avg																					
			0.58	0.96	0.61	0.05	0.18	0.08	0.00	0.00	0.00	0.81	1.24	0.83	0.00	0.00	0.00	0.00	0.00	0.00	0.00	0.00	0.00	0.00	0.00	0.00	0.00	0.00	0.00	0.00	0.00	0.00	0.00	0.00	0.00						
✓			0.63	1.04	0.65	0.05	0.20	0.09	-3.67	-3.55	-2.79	0.84	1.30	0.86	0.00	0.00	0.00	0.00	0.00	0.00	-1.57	-2.06	-1.54	0.80	1.13	0.80	0.00	0.00	0.00	1.05	3.78	1.54	0.77	1.10	0.78	0.00	0.00	0.00	2.10	4.81	2.56
	✓		0.41	0.75	0.43	0.05	0.22	0.09	12.49	9.32	12.58	0.72	1.04	0.74	0.00	0.00	0.00	0.00	0.00	0.00	5.26	6.87	4.62	0.72	1.04	0.74	0.00	0.00	0.00	0.00	0.00	0.00	0.00	0.00	0.00	0.00	0.00	0.00	0.00	0.00	
		✓	0.38	0.69	0.39	0.03	0.14	0.06	14.70	11.99	14.68	0.72	1.04	0.74	0.00	0.00	0.00	0.00	0.00	0.00	5.26	6.87	4.62	0.72	1.04	0.74	0.00	0.00	0.00	0.00	0.00	0.00	0.00	0.00	0.00	0.00	0.00	0.00	0.00	0.00	

varied driving scenarios, underscoring TTOG’s potential as a foundational framework for next-generation autonomous vehicles.

In Bench2Drive-fs and nuScenes-fs (Open-Loop), Table 3 summarizes the planning performance on the NuScenes-fs and Bench2Drive-fs validation datasets, evaluating key metrics: L2 error and collision rate. We compare TTOG with SparseDrive (baseline), VAD and UniAD(prior state-of-the-art). The results demonstrate TTOG’s effectiveness in few-shot driving scenarios, particularly in balancing prediction precision and safety. *In NuScene-fs*, TTOG achieves significant improvements over baseline. It reduces the average L2 error to 0.80, outperforming SparseDrive (0.99, 19% reduction) and VAD (1.20, 33% reduction). Notably, TTOG also lowers the collision rate to 0.03, a 3× and 15.7× improvement over SparseDrive (0.09) and VAD (0.47), respectively. These gains arise from TTOG’s integration of motion data during training, which alleviates data scarcity in few-shot planning. *In Bench2Drive-fs*, While the improvements are

less pronounced, TTOG still achieves a 0.07 reduction in L2 error compared to SparseDrive. This smaller margin likely stems from Bench2Drive-FS’s inherent bias toward scene allocation and its limited few-shot instances, which diminish the impact of TTOG’s motion-augmented training. Nevertheless, TTOG maintains a 0.00 collision rate, surpassing all other methods and underscoring its robustness in safety-critical planning. Overall, TTOG consistently outperforms other methods by effectively utilizing motion data for few-shot planning. Its joint optimization of motion and planning tasks improves both accuracy and safety, especially in NuScenes-fs and Bench2Drive-fs.

4.3 Ablation Study

4.3.1 The roles of different modules in TTOG

On the NuScenes and Bench2Drive Datasets: Table 6 presents ablation studies of the TTOG model on NuScenes and Bench2Drive datasets, analyzing the impact of different

TABLE 7: Ablation studies of the impact of the different modules in TTOG on the NuScenes-fs [44] and Bench2Drive-fs [45] validation datasets. UMP stands for the unified output of motion and planning in a simplified manner. ESCA denotes Equivariant Context-Sharing Scene Adapter module, TTOG denotes Unified Two-Stage Trajectory Decoder. **Blue** represents positive improvement, and **Red** represents negative improvement.

UMP	ESCA	UTTD	NuScene-fs									Bench2Drive-fs								
			L2(m)			Col.Rate(%)			CEGR(L2)			L2(m)			Col.Rate(%)			CEGR(L2)		
			2s	3s	Avg	2s	3s	Avg	2s	3s	Avg	2s	3s	Avg	2s	3s	Avg	2s	3s	Avg
			0.59	0.99	0.63	0.00	0.29	0.09	0.00	0.00	0.00	0.82	1.68	0.98	0.00	0.00	0.00	0.00	0.00	0.00
✓			0.64	1.09	0.68	0.00	0.30	0.09	-3.61	-4.30	-3.38	0.82	1.77	1.01	0.00	0.00	0.00	0.00	-2.28	-1.30
	✓		0.57	0.94	0.60	0.00	0.29	0.09	1.44	2.15	2.03	0.80	1.63	0.95	0.00	0.00	0.00	1.04	1.26	1.30
		✓	0.44	0.83	0.48	0.00	0.16	0.05	10.84	6.89	10.15	0.76	1.37	0.86	0.00	0.00	0.00	3.12	7.86	5.22
	✓	✓	0.39	0.80	0.45	0.00	0.09	0.03	14.40	8.18	12.18	0.75	1.31	0.84	0.00	0.00	0.00	3.64	9.39	6.09

TABLE 8: Ablation studies of the impact of the different modules in TTOG on the Bench2Drive Close-Loop [45] validation dataset. UMP stands for the unified output of motion and planning in a simplified manner. ESCA denotes Equivariant Context-Sharing Scene Adapter module, TTOG denotes Unified Two-Stage Trajectory Decoder. **Blue** represents positive improvement, and **Red** represents negative improvement.

UMP	ESCA	UTTD	Drive Score	Success Rate	CEGR (DS)	CEGR (SR)
			42.12	15.00	0.00	0.00
✓			38.70	10.00	-3.46	-14.21
	✓		42.35	15.00	0.63	0.00
		✓	44.70	15.45	2.71	1.27
	✓	✓	45.35	16.36	3.27	3.86

TABLE 9: The ablation study of motion data for improving TTOG performance on NuScenes validation dataset. **Blue** represents positive improvement, and **Red** represents negative improvement.

Epoch	Motion Volume	Method (Avg.)				CEGR(L2)
		TTOG		SparseDrive		
		L2	Col.Rate	L2	Col.Rate	
1	1632	1.98	0.16	2.83	0.37	11.02
2	3426	0.49	0.14	1.44	0.61	24.96
3	5019	0.49	0.10	0.95	0.26	18.05
4	6902	0.45	0.09	0.88	0.21	18.57
5	8851	0.42	0.10	0.83	0.21	19.07
6	10693	0.41	0.09	0.80	0.16	18.90
7	12498	0.40	0.06	0.75	0.12	18.11
8	14420	0.40	0.06	0.65	0.09	15.02
9	16099	0.39	0.06	0.64	0.07	15.18
10	17793	0.39	0.06	0.61	0.08	13.18

modules (UMP, ESCA, and UTTD) on performance metrics including L2 (m), Col. Rate, and CEGR (L2). UMP module streamlines model architecture by unifying motion and planning tasks. However, empirical results reveal suboptimal performance on NuScenes, particularly in L2 (m) and CEGR (L2) metrics. This indicates that a simplistic unification of tasks fails to account for the inherent disparities between motion and planning tasks, consequently resulting in performance degradation. With the introduction of the ESCA module, TTOG demonstrates significant improvements on both the Bench2Drive and NuScenes datasets. Particularly on the NuScenes dataset, at $t = 2$, the L2(m) error decreases to 0.51 m, the collision rate (Col. Rate) drops to 0.22%, and the CEGR(avg) reaches 4.89. The ESCA module unifies perspectives through equivariant operations, enabling the model to better learn from motion data. With

the introduction of the UTTD module, the overall performance of TTOG has been further significantly improved. On the NuScenes dataset and Bench2Drive, the CEGR (L2) reached 12.58 and 2.56, respectively, demonstrating the model’s strong capability in motion learning and trajectory prediction. Compared to other modules, UTTD effectively unifies motion and planning tasks, leading to a notable enhancement in model performance.

On the NuScenes-fs and Bench2Drive-fs Datasets: Table 7 presents the ablation study results of the TTOG model on the NuScenes-fs and Bench2Drive-fs datasets. The experiments analyze the impact of different modules (UMP, ESCA, and UTTD) on key metrics including L2 (m), Col. Rate, and CEGR (L2). The UMP module simplifies model architecture by unifying motion and planning tasks. However, its performance proves unsatisfactory on both few-shot datasets, particularly in CEGR (L2) metrics. On NuScenes-fs and Bench2Drive at $t=2s$, UMP achieves CEGR (L2) of -4.30 and -2.28, indicating significant difficulties in motion learning. This limitation stems from UMP’s failure to account for inherent task differences and perspective variations, impairing few-shot adaptation. The ESCA leverages equivariant operations to enhance motion learning and viewpoint adaptation, achieving 0.57m L2, 0.18% (Col. Rate), and -2.53 (CEGR) on NuScenes-fs ($t=2s$). The UTTD unifies motion and planning while preserving task distinctions, delivering superior performance (AVG) 0.77m (L2), 0.0% (Col. Rate), 4.62 (CEGR). Full integration maintains TTOG’s optimal metrics, demonstrating that ESCA’s adaptation capabilities and UTTD’s task-aware design synergistically improve few-shot learning for both motion and planning tasks. And full integration maintains TTOG’s optimal metrics, demonstrating that ESCA’s adaptation capabilities and UTTD’s task-aware design synergistically improve few-shot learning for both motion and planning tasks.

On the Bench2Drive (Close-Loop) Dataset: As shown in Table 8, our systematic evaluation examines TTOG’s performance through four key metrics: Success Rate (SR), Drive Score (DS), and CEGR(DS)/CEGR(SR) that quantify motion data learning capabilities for route completion and driving quality. The unified approach, UMP, shows limited closed-loop effectiveness (SR: 38.70%, DS: 10.00, CEGR (SR): -3.46, CEGR (DS): -14.21), revealing fundamental limitations in handling temporal, distributional, and perspective differences between motion and planning tasks. The ESCA module demonstrates measurable improvements (SR: 42.35%, DS: 15.00, CEGR (SR): 0.63, CEGR (DS): 0.00), confirming its

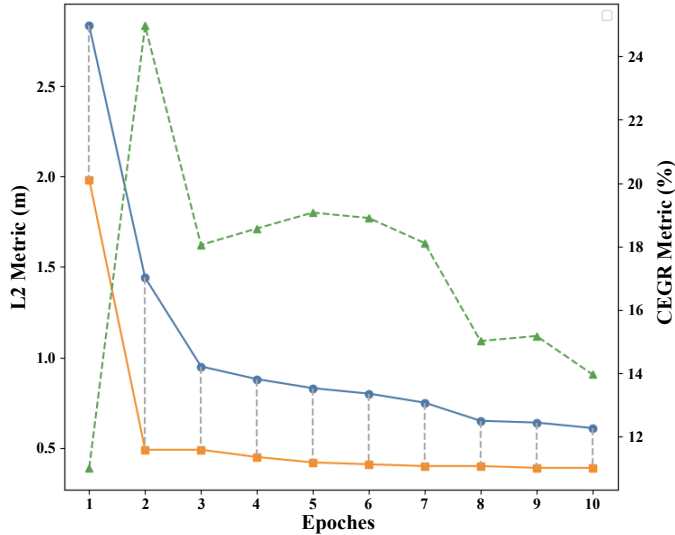


Fig. 4: The visualization of the convergence of SparseDrive and TTOG, as well as the visualization of CEGR changing with motion data volume.

effectiveness in mitigating viewpoint variations for better generalization. And UTDD module achieves superior trajectory prediction (SR: 44.70%, DS: 15.45, CEGR (SR): 2.71, CEGR (DS): 1.27), validating its task-aware unification strategy for enhanced motion and plan understanding. Nobaly, The combined modules deliver state-of-the-art performance (SR: 45.35%, DS: 16.36, CEGR (SR): 3.27, CEGR (DS): 3.86) and demonstrates synergistic benefits: ESCA’s perspective robustness complements and UTDD’s structured task unification for reliable real-world driving.

4.3.2 The effect of motion data volume in TTOG

Based on Table 9 and Fig. 4, the experiment demonstrates the impact of different volumes of motion data on the performance of the model. The results indicate that TTOG, which is capable of learning from motion data, shows rapid convergence and significant performance improvements early in the training process. Specifically, after only two epochs, TTOG reaches a notable level of performance, as indicated by a substantial reduction in L2 and Col.Rate. On the other hand, SparseDrive, which does not have the ability to learn from motion data, exhibits slower convergence during the training period. It takes until the final epoch to reach its optimal performance. In comparison, TTOG converges to a near-optimal performance level by epoch 6, showcasing its superior ability to leverage motion data and convert them into useful plan data.

Otherwise, in the first two epochs, the CEGR of the TTOG model exhibits a significant improvement as the volume of motion data increases. In particular, when the motion volume expands from 1,632 to 3,426, the CEGR rises sharply from 11.02 to 24.96. With further increments in motion volume, the CEGR stabilizes around 19.07 by Epoch 6 and remains stable thereafter. This shows that TTOG efficiently leverages motion data for early-stage optimization and achieves high performance with rapid convergence.

5 VISUALIZATION

We visualize TTOG’s performance on NuScene-fs and Bench2Drive-fs, focusing on few-shot driving scenarios. For NuScene-fs, we select four scenarios that involve turning and lane change, while Bench2Drive-fs includes turning, lane change, and brake. As shown in Fig. 6 and Fig. 5, TTOG achieves robust performance in all data sets of a few shots, particularly in brake and lane change scenarios. This highlights its capability to effectively transfer knowledge from other vehicles’ data to enhance its own driving skills.

6 CONCLUSION

In this work, we propose TTOG, an end-to-end autonomous driving framework that leverages motion data to enhance the model’s learning capacity and improve few-shot performance. Specifically, TTOG employs a graph-based equivariant structure to unify the observational perspectives of both ego and other vehicles, ensuring cross-vehicle viewpoint consistency. We further introduce a novel decoder architecture to jointly optimize motion prediction and planning tasks. For evaluation, we construct a few-shot benchmark by subsampling the NuScenes and Bench2Drive validation sets. Extensive experiments demonstrate that TTOG significantly outperforms state-of-the-art end-to-end methods in trajectory prediction. Our work aims to advance the community’s understanding of motion data utilization and its benefits for planning tasks.

Limitation and future work. Although TTOG effectively unifies motion planning and trajectory optimization tasks, its vehicle state estimator demonstrates limited reliability in handling occluded or sensor-missing scenarios, particularly for surrounding vehicles with incomplete modality inputs. This limitation motivates our future research focus on robust multi-agent state estimation under perceptual uncertainty.

ACKNOWLEDGMENTS

This work was supported in part by the National Key R&D Program of China (2018AAA0100302), supported by the STI 2030-Major Projects under Grant 2021ZD0201404.

REFERENCES

- [1] Y. Hu, J. Yang, L. Chen, K. Li, C. Sima, X. Zhu, S. Chai, S. Du, T. Lin, W. Wang, L. Lu, X. Jia, Q. Liu, J. Dai, Y. Qiao, and H. Li, “Planning-oriented autonomous driving,” in *Proceedings of the IEEE/CVF Conference on Computer Vision and Pattern Recognition (CVPR)*, June 2023, pp. 17853–17862.
- [2] W. Sun, X. Lin, Y. Shi, C. Zhang, H. Wu, and S. Zheng, “Sparsedrive: End-to-end autonomous driving via sparse scene representation,” *arXiv preprint arXiv:2405.19620*, 2024.
- [3] B. Jiang, S. Chen, Q. Xu, B. Liao, J. Chen, H. Zhou, Q. Zhang, W. Liu, C. Huang, and X. Wang, “Vad: Vectorized scene representation for efficient autonomous driving,” in *Proceedings of the IEEE/CVF International Conference on Computer Vision*, 2023, pp. 8340–8350.
- [4] S. Chen, B. Jiang, H. Gao, B. Liao, Q. Xu, Q. Zhang, C. Huang, W. Liu, and X. Wang, “Vadv2: End-to-end vectorized autonomous driving via probabilistic planning,” *arXiv preprint arXiv:2402.13243*, 2024.

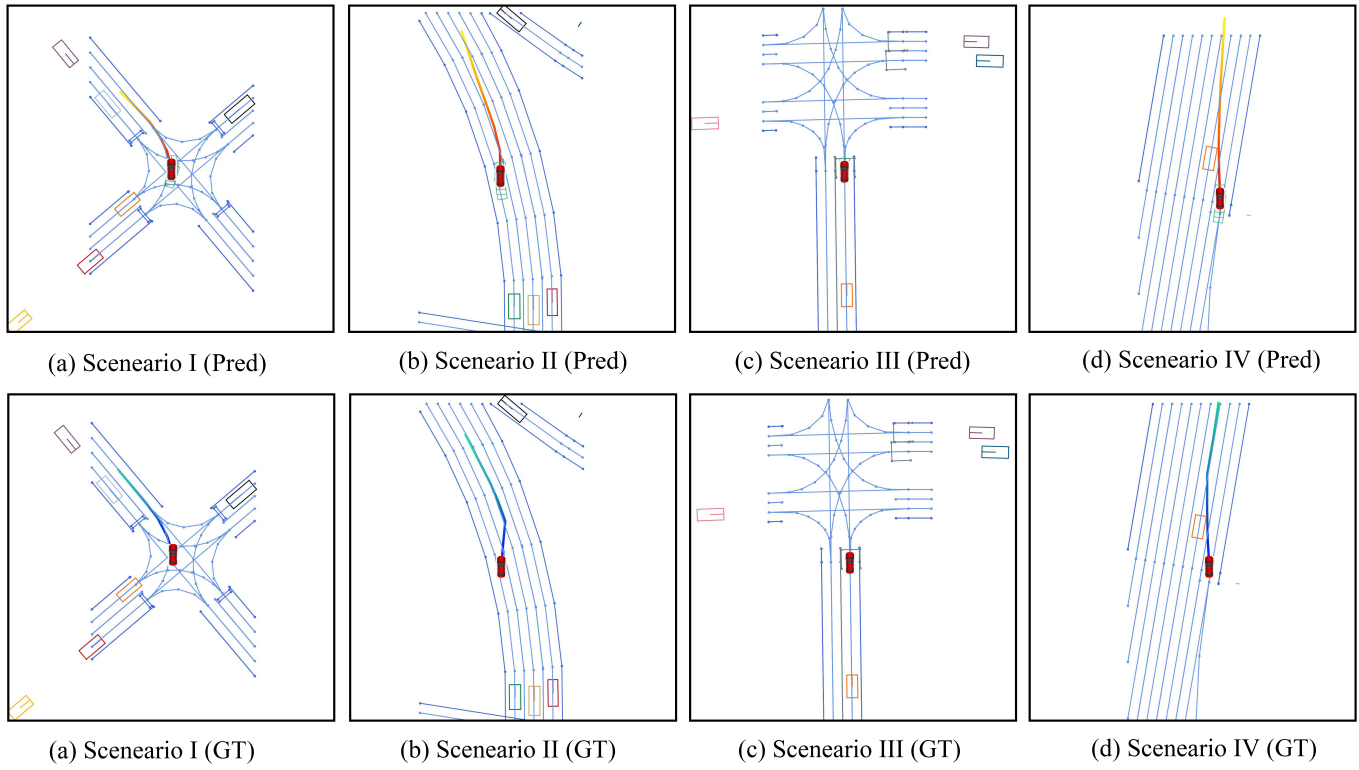


Fig. 5: The visualization results of TTOG with GT on NuScene-fs Dataset. Four scenarios encompass: turning (a), lane change (b), (d) and brake (c).

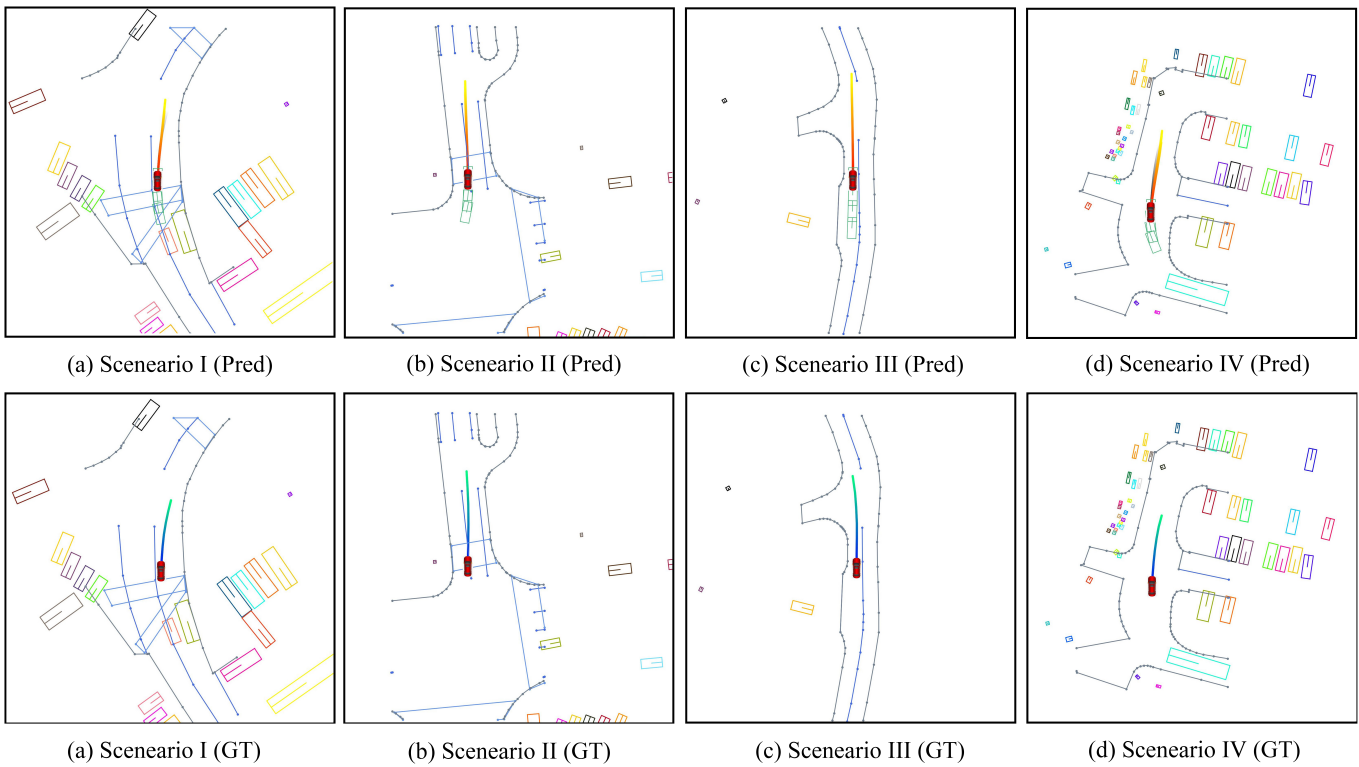
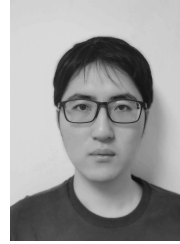


Fig. 6: The visualization results of TTOG with GT on Bench2Drive-fs Dataset. Four scenarios encompass: turning (a), (b), (c), and lane change (d).

- [5] J. Cheng, Y. Chen, X. Mei, B. Yang, B. Li, and M. Liu, "Rethinking imitation-based planners for autonomous driving," in *2024 IEEE International Conference on Robotics and Automation (ICRA)*. IEEE, 2024, pp. 14 123–14 130.
- [6] M. Guo, Z. Zhang, Y. He, K. Wang, and L. Jing, "End-to-end autonomous driving without costly modularization and 3d manual annotation," *arXiv preprint arXiv:2406.17680*, 2024.
- [7] X. Jia, Y. Gao, L. Chen, J. Yan, P. L. Liu, and H. Li, "Driveadapter: Breaking the coupling barrier of perception and planning in end-to-end autonomous driving," in *Proceedings of the IEEE/CVF International Conference on Computer Vision*, 2023, pp. 7953–7963.
- [8] W. Zheng, R. Song, X. Guo, and L. Chen, "Genad: Generative end-to-end autonomous driving," *arXiv preprint arXiv:2402.11502*, 2024.
- [9] X. Jia, P. Wu, L. Chen, J. Xie, C. He, J. Yan, and H. Li, "Think twice before driving: Towards scalable decoders for end-to-end autonomous driving," in *Proceedings of the IEEE/CVF Conference on Computer Vision and Pattern Recognition (CVPR)*, June 2023, pp. 21 983–21 994.
- [10] N. Rhinehart, J. He, C. Packer, M. A. Wright, R. McAllister, J. E. Gonzalez, and S. Levine, "Contingencies from observations: Tractable contingency planning with learned behavior models," in *2021 IEEE International Conference on Robotics and Automation (ICRA)*. IEEE, 2021, pp. 13 663–13 669.
- [11] A. Cui, S. Casas, A. Sadat, R. Liao, and R. Urtasun, "Lookout: Diverse multi-future prediction and planning for self-driving," in *2021 IEEE/CVF International Conference on Computer Vision (ICCV)*, Oct 2021. [Online]. Available: <http://dx.doi.org/10.1109/iccv48922.2021.01580>
- [12] J. Hardy and M. Campbell, "Contingency planning over probabilistic obstacle predictions for autonomous road vehicles," *IEEE Transactions on Robotics*, p. 913–929, Aug 2013. [Online]. Available: <http://dx.doi.org/10.1109/tro.2013.2254033>
- [13] J. F. Fisac, E. Bronstein, E. Stefansson, D. Sadigh, S. S. Sastry, and A. D. Dragan, "Hierarchical game-theoretic planning for autonomous vehicles," in *2019 International Conference on Robotics and Automation (ICRA)*, May 2019. [Online]. Available: <http://dx.doi.org/10.1109/icra.2019.8794007>
- [14] H. Su, W. Wu, and J. Yan, "Difsd: Ego-centric fully sparse paradigm with uncertainty denoising and iterative refinement for efficient end-to-end autonomous driving," *arXiv preprint arXiv:2409.09777*, 2024.
- [15] Z. Huang, H. Liu, and C. Lv, "Gameformer: Game-theoretic modeling and learning of transformer-based interactive prediction and planning for autonomous driving," in *Proceedings of the IEEE/CVF International Conference on Computer Vision*, 2023, pp. 3903–3913.
- [16] J. Wright and K. Leyton-Brown, "Beyond equilibrium: Predicting human behavior in normal-form games," *Proceedings of the AAAI Conference on Artificial Intelligence*, p. 901–907, Sep 2022. [Online]. Available: <http://dx.doi.org/10.1609/aaai.v24i1.7644>
- [17] Y. Chen, B. Ivanovic, and M. Pavone, "Scept: Scene-consistent, policy-based trajectory predictions for planning," in *Proceedings of the IEEE/CVF conference on computer vision and pattern recognition*, 2022, pp. 17 103–17 112.
- [18] K. Kinningham, P. Levis, and C. Ré, "Grip: A graph neural network accelerator architecture," *IEEE Transactions on Computers*, vol. 72, no. 4, pp. 914–925, 2022.
- [19] J. Gu, C. Sun, and H. Zhao, "Densetnt: End-to-end trajectory prediction from dense goal sets," in *Proceedings of the IEEE/CVF International Conference on Computer Vision*, 2021, pp. 15 303–15 312.
- [20] X. Li, X. Ying, and M. C. Chuah, "Grip++: Enhanced graph-based interaction-aware trajectory prediction for autonomous driving," *arXiv preprint arXiv:1907.07792*, 2019.
- [21] Y. Liu, J. Zhang, L. Fang, Q. Jiang, and B. Zhou, "Multimodal motion prediction with stacked transformers," in *2021 IEEE/CVF Conference on Computer Vision and Pattern Recognition (CVPR)*, Jun 2021. [Online]. Available: <http://dx.doi.org/10.1109/cvpr46437.2021.00749>
- [22] L. L. Li, B. Yang, M. Liang, W. Zeng, M. Ren, S. Segal, and R. Urtasun, "End-to-end contextual perception and prediction with interaction transformer," in *2020 IEEE/RSJ International Conference on Intelligent Robots and Systems (IROS)*, Oct 2020. [Online]. Available: <http://dx.doi.org/10.1109/iro545743.2020.9341392>
- [23] C. Min, D. Zhao, L. Xiao, J. Zhao, X. Xu, Z. Zhu, L. Jin, J. Li, Y. Guo, J. Xing *et al.*, "Driveworld: 4d pre-trained scene understanding via world models for autonomous driving," in *Proceedings of the IEEE/CVF Conference on Computer Vision and Pattern Recognition*, 2024, pp. 15 522–15 533.
- [24] S. Pini, C. S. Perone, A. Ahuja, A. S. R. Ferreira, M. Nien-dorf, and S. Zagoruyko, "Safe real-world autonomous driving by learning to predict and plan with a mixture of experts," in *2023 IEEE International Conference on Robotics and Automation (ICRA)*. IEEE, 2023, pp. 10 069–10 075.
- [25] F. Codevilla, M. Müller, A. López, V. Koltun, and A. Dosovitskiy, "End-to-end driving via conditional imitation learning," in *2018 IEEE International Conference on Robotics and Automation (ICRA)*, 2018, pp. 4693–4700.
- [26] F. Codevilla, E. Santana, A. M. Lopez, and A. Gaidon, "Exploring the limitations of behavior cloning for autonomous driving," in *Proceedings of the IEEE/CVF International Conference on Computer Vision (ICCV)*, October 2019.
- [27] P. Wu, X. Jia, L. Chen, J. Yan, H. Li, and Y. Qiao, "Trajectory-guided control prediction for end-to-end autonomous driving: A simple yet strong baseline," in *Advances in Neural Information Processing Systems*, S. Koyejo, S. Mohamed, A. Agarwal, D. Belgrave, K. Cho, and A. Oh, Eds., vol. 35. Curran Associates, Inc., 2022, pp. 6119–6132. [Online]. Available: https://proceedings.neurips.cc/paper_files/paper/2022/file/286a371d8a0a559281f682f8fbf89834-Paper-Conference.pdf
- [28] Z. Zhang, A. Liniger, D. Dai, F. Yu, and L. Van Gool, "End-to-end urban driving by imitating a reinforcement learning coach," in *Proceedings of the IEEE/CVF International Conference on Computer Vision (ICCV)*, October 2021, pp. 15 222–15 232.
- [29] K. Chitta, A. Prakash, B. Jaeger, Z. Yu, K. Renz, and A. Geiger, "Transfuser: Imitation with transformer-based sensor fusion for autonomous driving," *IEEE Transactions on Pattern Analysis and Machine Intelligence*, vol. 45, no. 11, pp. 12 878–12 895, 2023.
- [30] J. Mao, Y. Qian, H. Zhao, and Y. Wang, "Gpt-driver: Learning to drive with gpt," *arXiv preprint arXiv:2310.01415*, 2023.
- [31] H. Shao, L. Wang, R. Chen, H. Li, and Y. Liu, "Safety-enhanced autonomous driving using interpretable sensor fusion transformer," in *Proceedings of The 6th Conference on Robot Learning*, ser. Proceedings of Machine Learning Research, K. Liu, D. Kulic, and J. Ichnowski, Eds., vol. 205. PMLR, 14–18 Dec 2023, pp. 726–737. [Online]. Available: <https://proceedings.mlr.press/v205/shao23a.html>
- [32] H. Shao, L. Wang, R. Chen, S. L. Waslander, H. Li, and Y. Liu, "Reasonnet: End-to-end driving with temporal and global reasoning," in *Proceedings of the IEEE/CVF conference on computer vision and pattern recognition*, 2023, pp. 13 723–13 733.
- [33] D. Xu, H. Li, Q. Wang, Z. Song, L. Chen, and H. Deng, "M2da: Multi-modal fusion transformer incorporating driver attention for autonomous driving," *arXiv preprint arXiv:2403.12552*, 2024.
- [34] Z. Chen, M. Ye, S. Xu, T. Cao, and Q. Chen, "Ppad: Iterative

- interactions of prediction and planning for end-to-end autonomous driving," in *European Conference on Computer Vision*. Springer, 2025, pp. 239–256.
- [35] S. Doll, N. Hanselmann, L. Schneider, R. Schulz, M. Cordts, M. Enzweiler, and H. Lensch, "Dualad: Disentangling the dynamic and static world for end-to-end driving," in *Proceedings of the IEEE/CVF Conference on Computer Vision and Pattern Recognition*, 2024, pp. 14728–14737.
- [36] B. Jiang, S. Chen, B. Liao, X. Zhang, W. Yin, Q. Zhang, C. Huang, W. Liu, and X. Wang, "Senna: Bridging large vision-language models and end-to-end autonomous driving," 2024. [Online]. Available: <https://arxiv.org/abs/2410.22313>
- [37] J. Wang, X. Zhang, Z. Xing, S. Gu, X. Guo, Y. Hu, Z. Song, Q. Zhang, X. Long, and W. Yin, "He-drive: Human-like end-to-end driving with vision language models," 2024. [Online]. Available: <https://arxiv.org/abs/2410.05051>
- [38] T. Ye, W. Jing, C. Hu, S. Huang, L. Gao, F. Li, J. Wang, K. Guo, W. Xiao, W. Mao, H. Zheng, K. Li, J. Chen, and K. Yu, "Fusionad: Multi-modality fusion for prediction and planning tasks of autonomous driving," 2023. [Online]. Available: <https://arxiv.org/abs/2308.01006>
- [39] Z. Yang, N. Song, W. Li, X. Zhu, L. Zhang, and P. H. Torr, "Deepinteraction++: Multi-modality interaction for autonomous driving," *arXiv preprint arXiv:2408.05075*, 2024.
- [40] Y. Zhang, D. Qian, D. Li, Y. Pan, Y. Chen, Z. Liang, Z. Zhang, S. Zhang, H. Li, M. Fu *et al.*, "Graphad: Interaction scene graph for end-to-end autonomous driving," *arXiv preprint arXiv:2403.19098*, 2024.
- [41] Z. Huang, P. Karkus, B. Ivanovic, Y. Chen, M. Pavone, and C. Lv, "Dtpp: Differentiable joint conditional prediction and cost evaluation for tree policy planning in autonomous driving," in *2024 IEEE International Conference on Robotics and Automation (ICRA)*. IEEE, 2024, pp. 6806–6812.
- [42] C. R. Qi, H. Su, K. Mo, and L. J. Guibas, "Pointnet: Deep learning on point sets for 3d classification and segmentation," in *Proceedings of the IEEE conference on computer vision and pattern recognition*, 2017, pp. 652–660.
- [43] B. Liao, S. Chen, B. Jiang, T. Cheng, Q. Zhang, W. Liu, C. Huang, and X. Wang, "Lane graph as path: Continuity-preserving path-wise modeling for online lane graph construction," *arXiv preprint arXiv:2303.08815*, 2023.
- [44] H. Caesar, V. Bankiti, A. H. Lang, S. Vora, V. E. Liong, Q. Xu, A. Krishnan, Y. Pan, G. Baldan, and O. Beijbom, "nuscenes: A multimodal dataset for autonomous driving," in *Proceedings of the IEEE/CVF conference on computer vision and pattern recognition*, 2020, pp. 11 621–11 631.
- [45] X. Jia, Z. Yang, Q. Li, Z. Zhang, and J. Yan, "Bench2drive: Towards multi-ability benchmarking of closed-loop end-to-end autonomous driving."
- [46] N. D. Ratliff, J. A. Bagnell, and M. A. Zinkevich, "Maximum margin planning," in *Proceedings of the 23rd international conference on Machine learning*, 2006, pp. 729–736.
- [47] W. Zeng, W. Luo, S. Suo, A. Sadat, B. Yang, S. Casas, and R. Urtasun, "End-to-end interpretable neural motion planner," in *Proceedings of the IEEE/CVF Conference on Computer Vision and Pattern Recognition*, 2019, pp. 8660–8669.
- [48] P. Hu, A. Huang, J. Dolan, D. Held, and D. Ramanan, "Safe local motion planning with self-supervised freespace forecasting," in *Proceedings of the IEEE/CVF Conference on Computer Vision and Pattern Recognition*, 2021, pp. 12732–12741.
- [49] T. Khurana, P. Hu, A. Dave, J. Ziglar, D. Held, and D. Ramanan, "Differentiable raycasting for self-supervised occupancy forecasting," in *European Conference on Computer Vision*. Springer, 2022, pp. 353–369.
- [50] S. Hu, L. Chen, P. Wu, H. Li, J. Yan, and D. Tao, "St-p3: End-to-end vision-based autonomous driving via spatial-temporal feature learning," in *European Conference on Computer Vision*. Springer, 2022, pp. 533–549.
- [51] W. Tong, C. Sima, T. Wang, L. Chen, S. Wu, H. Deng, Y. Gu, L. Lu, P. Luo, D. Lin *et al.*, "Scene as occupancy," in *Proceedings of the IEEE/CVF International Conference on Computer Vision*, 2023, pp. 8406–8415.



Lin Liu was born in Jinzhou, Liaoning Province, China, in 2001. He is now a college student majoring in Computer Science and Technology at China University of Geosciences(Beijing). Since Dec. 2022, he has been recommended for a master's degree in Computer Science and Technology at Beijing Jiaotong University. His research interests are in computer vision.



Ziyang Song, was born in Xingtai, Hebei Province, China in 1997. He received the B.S. degree from Hebei Normal University of Science and Technology (China) in 2019. He received a master's degree major in Hebei University of Science and Technology (China) in 2022. He is now a PhD student majoring in Computer Science and Technology at Beijing Jiaotong University (China), with a research focus on Computer Vision.



Hongyu Pan received the B.E. degree from Beijing Institute of Technology (BIT) in 2016 and the M.S. degree in computer science from the Institute of Computing Technology (ICT), University of Chinese Academy of Sciences (UCAS), in 2019. He is currently an employee at Horizon Robotics. His research interests include computer vision, pattern recognition, and image processing. He specifically focuses on 3D detection/segmentation/motion and depth estimation.



Lei Yang (Graduate Student Member, IEEE) received his B.E. degree from Taiyuan University of Technology, Taiyuan, China, and the M.S. degree from the Robotics Institute at Beihang University, in 2018. Then he joined the Autonomous Driving R&D Department of JD.COM as an algorithm researcher from 2018 to 2020. He is now a Ph.D. student in the School of Vehicle and Mobility at Tsinghua University since 2020. His current research interests include computer vision, 3D scene understanding and autonomous driving.



Caiyan Jia, born on March 2, 1976, is a lecturer and a postdoctoral fellow of the Chinese Computer Society. she graduated from Ningxia University in 1998 with a bachelor's degree in mathematics, Xiangtan University in 2001 with a master's degree in computational mathematics, specializing in intelligent information processing, and the Institute of Computing Technology of the Chinese Academy of Sciences in 2004 with a doctorate degree in engineering, specializing in data mining. she has received her D. degree in 2004. She is now a professor in School of Computer Science and Technology, Beijing Jiaotong University, Beijing, China.